tvst

Article

Visualization of Anterior Chamber Angle Structures With Scattering- and Polarization-Sensitive Anterior Segment Optical Coherence Tomography

Yuta Ueno[1,*], Haruhiro Mori[1,*], Keita Kikuchi[1], Masahiro Yamanari[2], and Tetsuro Oshika[1]

[1] Department of Ophthalmology, Faculty of Medicine, University of Tsukuba, Ibaraki, Japan
[2] Department of Technological Development, Tomey Corporation, Nagoya, Japan

Correspondence: Tetsuro Oshika, Department of Ophthalmology, Faculty of Medicine, University of Tsukuba, 1-1-1 Tennoudai, Tsukuba, Ibaraki 305-8575, Japan.
e-mail: oshika@eye.ac

Received: September 14, 2021
Accepted: December 2, 2021
Published: December 29, 2021

Keywords: OCT; polarization; anterior chamber angle

Citation: Ueno Y, Mori H, Kikuchi K, Yamanari M, Oshika T. Visualization of anterior chamber angle structures with scattering- and polarization-sensitive anterior segment optical coherence tomography. Transl Vis Sci Technol. 2021;10(14):29, https://doi.org/10.1167/tvst.10.14.29

Purpose: The purpose of this study was to compare three optical coherence tomography (OCT) modalities in the observation of anterior chamber angle structures; trabecular meshwork (TM), Schlemm's canal (SC), and band of extracanalicular limbal lamina (BELL).

Methods: Three OCT modalities were used: (1) 2 × 2 Jones-matrix scattering OCT (S-OCT) representing conventional intensity OCT, (2) polarization-diverse S-OCT that was calculated as summation of all elements of the Jones-matrix to eliminate the influence of artifacts caused by sample birefringence, and (3) polarization-sensitive OCT (PS-OCT) to assess depth-resolved phase retardation.

Results: In a total of 97 eyes of 55 subjects, nasal and temporal angles were scanned. The detection rate of TM and BELL was significantly different among modalities; highest with PS-OCT (95.1% and 99.2%), followed by 2 × 2 Jones-matrix S-OCT (71.1% and 88.7%) and polarization-diverse S-OCT (33.2% and 25.0%), indicating the influence of artifacts on 2 × 2 Jones-matrix S-OCT measurements. SC was visible with 2 × 2 Jones-matrix S-OCT, polarization-diverse S-OCT, and PS-OCT in 14.2%, 14.9%, and 0.3% of images, respectively. The intergrader agreement as evaluated with the prevalence-adjusted bias-adjusted κ value was higher with PS-OCT than with other S-OCTs.

Conclusions: Visibility of anterior chamber angle structures was assessed with three OCT modalities. For TM and BELL that are rich in collagen fibers, PS-OCT provides significantly better visibility than S-OCT without the influence of artifacts arising from polarization or birefringence. Visualization of SC was more difficult with any OCT modalities.

Translational Relevance: PS-OCT is a useful tool to investigate the anterior chamber angle structures which are difficult to observe with conventional OCT.

Introduction

Aqueous humor outflow occurs through two routes, the conventional (trabecular) and uveoscleral pathways. In human eyes, the conventional pathway is the main aqueous drainage route, and outflow resistance exists primarily within the cribriform or juxtacanalicular region of the trabecular meshwork (TM) and the inner wall of Schlemm's canal (SC).[1,2] With the development of new intraocular pressure (IOP) lowering drugs and minimally invasive glaucoma surgeries, renewed interests have been directed to the microstructures of the trabecular/conventional pathway.

Anterior segment optical coherence tomography (OCT) is a powerful tool for biological tissue scanning of the anterior chamber angle structures. Studies have shown that anterior segment OCT can noninvasively detect the TM and SC in healthy and pathological human eyes.[3–9] Recently, Crowell et al.[10] reported the presence of a novel anatomic landmark termed the band of extracanalicular limbal lamina (BELL) adjacent to SC visible on anterior segment OCT. The

Copyright 2021 The Authors

This work is licensed under a Creative Commons Attribution-NonCommercial-NoDerivatives 4.0 International License.

pathological analysis verified BELL as the avascular collagenous layers external to SC,[10] which corresponds to the area where the collagen bundles from the cornea meet the sclera as they also pass between SC and the vasculature. BELL appears to be the structure that previously has been identified as the TM shadow seen on anterior segment OCT.[11–13] On the other hand, the dark band surrounding TM shown on the conventional OCT image was reported to be an artifact arising from sample birefringence.[14]

Among optical engineers, it is widely known that the local birefringence can produce artifacts in intensity-based scattering OCT (S-OCT) images.[14,15] This is because S-OCT in its principle ignores the vectorial nature of light (polarization of light) for simplicity. The OCT signal intensity can be altered by the relative difference in the polarization states of the reference and probe beams due to the Arago-Fresnel laws for the interference of polarized light,[16–18] and this intensity alteration can create artificial contrast in S-OCT images.[14] Thus, there is a possibility that S-OCT images of BELL demonstrated by Crowell et al.[10] represent artifacts caused by local birefringence. Optically, such artifacts can be removed by implementing polarization-diverse detection[19] in S-OCT, which has often been used in cardiovascular and gastrointestinal clinical studies.[20,21] The polarization-diverse detection has also been used to measure phase retardation with polarization-sensitive OCT (PC-OCT),[22,23] which we use to revisit the contrast mechanisms of the OCT images at the anterior chamber angle structures in this study.

Polarization-sensitive OCT (PS-OCT), an extension of conventional OCT, measures and analyzes the polarization of light, thereby provides additional contrast, such as phase retardation caused by the birefringence of a sample.[22,23] The polarization state of light is altered along the axial depth when passing through collagenous tissues. This system draws advantages from the fact that several materials can change the state of polarized light, visualizing additional contrast that is not available with the conventional OCT, and providing quantitative information related to the polarization-dependent changes.[23] In other words, whereas conventional intensity OCT does not provide a tissue-specific contrast, causing an ambiguity with image interpretation, PS-OCT can analyze form birefringence observed in fibrous tissues that contain collagens with specific polarization properties. Because PS-OCT can be technically regarded as a superset of OCT implementations that include conventional OCT, it can also provide intensity images from the same raw dataset, enabling us to generate inherently co-registered images. Anterior segment PS-OCT has been applied for the investigation of the internal space of filtering blebs following trabeculectomy,[24–28] noninvasive visualization of TM,[14] and assessment of corneal tissue abnormality in keratoconus.[29–31]

We conducted the current study to compare three different OCT images in the observation of anterior chamber angle structures (TM, SC, and BELL) in healthy and glaucomatous human eyes; 2 × 2 Jones-matrix S-OCT that could be regarded as an emulation of conventional S-OCT, polarization-diverse S-OCT, and PS-OCT that reflects the magnitude of birefringence (local retardation).

Methods

Participants

Retrospective review of S-OCT and PS-OCT images was carried out at Tsukuba University Hospital. The study adhered to the tenets of the Declaration of Helsinki, and the institutional review board of Tsukuba University Hospital approved the study protocol. The committee waived the requirement for patient informed consent regarding the use of their medical record data in accordance with the regulations of the Japanese Guidelines for Epidemiologic Study issued by the Japanese Government. Clinical trial registration was not required owing to the observational nature of the study. All participants were at least 18 years old.

Anterior Segment OCT

Both S-OCT and local retardation images were measured simultaneously with a custom-built anterior segment PS-OCT system, which was based on Jones-matrix OCT using a probe beam in two input polarization states.[32,33] The system used swept-source OCT technology centered at a 1.3-µm wavelength with an operating speed of 100,000 A-scans per second. The axial and lateral resolutions were 10.6 and 29 µm in tissue, respectively. This PS-OCT acquired depth-resolved Jones matrix that has 2 × 2 complex matrix elements. The Jones matrix described the polarization property of the sample completely in an optically coherent manner,[22,23] and was used to calculate all the S-OCT and local retardation images.

Angle imaging with anterior segment PS-OCT was conducted in a bright examination room. Participants were instructed to focus on an external fixation light. After adjusting the participant's position, eyes were scanned with a raster volumetric scan of 12 × 12 mm^2 (800 × 128 A-scans). The examiner viewed each scan

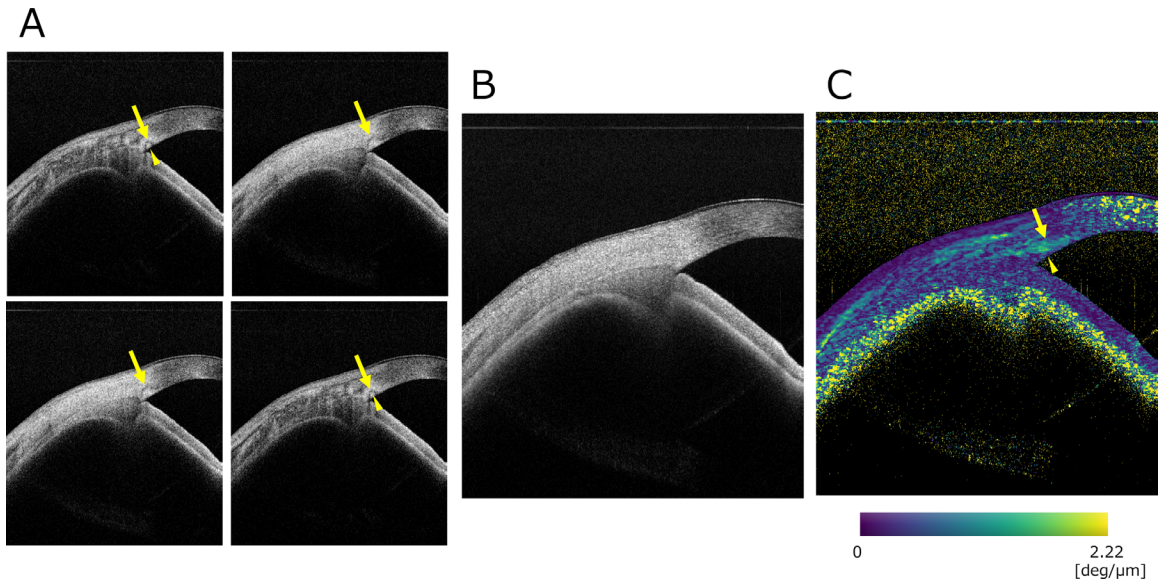

Figure 1. Three forms of OCT images were processed. (**A**) Four elements of 2 × 2 Jones matrix represent scattering-OCT (S-OCT) images (1A). Because of mathematical property of Jones-matrix for birefringent materials, the artifacts arising from local birefringence are unavoidable. Band of extracanalicular limbal lamina (BELL)-like structure (hyporeflective band-shaped area, *arrow*) and trabecular meshwork (TM) (surrounded by BELL, *arrow head*) are visible. (**B**) Polarization-diverse S-OCT image was calculated as a summation of all elements of the Jones-matrix. This image reflects the true backscattered signal intensity of the target without any influence of polarization or birefringence. (**C**) The depth-resolved local retardation image shows a magnitude of the local birefringence, which was referred to as polarization-sensitive OCT (PS-OCT). BELL (high birefringence band-shaped area, arrow) and TM (low birefringence area surrounded by BELL, *arrow head*) are observed.

to ensure that the image quality was acceptable, and a central B-scan of the first acceptable volume was used for the subsequent analyses.

Image Processing

Obtained images were processed to provide three forms of OCT images as follows (Fig. 1). First, 4 logarithmic intensity images were calculated from the 4 individual elements of the measured 2 × 2 Jones-matrix (see Fig. 1A).[14,15] These intensity images, which was called 2 × 2 Jones-matrix S-OCT in this study, represented polarization-dependent responses of light scattering intensity. The first and second columns showed the responses to horizontally and vertically polarized incident lights, respectively. The first and second rows showed horizontally and vertically polarized components of the backscattered lights from the sample, respectively. Because of a mathematical property of Jones matrix for birefringent materials that have negligible diattenuation, a pair of diagonal elements or off-diagonal elements of Jones matrix showed similar intensity signals, respectively. The signal intensity could be arbitrarily split to the first and second rows of the 2 × 2 Jones-matrix S-OCT, because stress-induced birefringence caused by bent single-mode optical fibers could change the state of polarization and thus the measured Jones matrix in our implementation of the interferometer. Of note, in the case of conventional S-OCT, only one element of the 2 × 2 Jones-matrix S-OCT can be detected,[22,23] and it was necessary to maximize the signal intensity of the detected element of Jones matrix, which was typically aligned using a polarization controller in the reference arm of the interferometer. Irrespective of the alignment, however, the artifacts arising from birefringence of the sample were unavoidable in each element of the 2 × 2 Jones-matrix S-OCT, because cumulative effect of the birefringence along the depth was always accompanied by the alteration of intensity in each element of Jones matrix except for a rare case where an optic axis of cumulative birefringence exactly corresponded to the horizontal or vertical axes. The 2 × 2 Jones-matrix S-OCT could therefore be regarded as an emulation of the conventional S-OCT.

Second, polarization-diverse S-OCT image was calculated as a summation of all elements of the Jones-matrix (see Fig. 1B).[22,23] Mathematically, this was equivalent to the first element of Mueller matrix with a constant coefficient and was known to represent the polarization-insensitive intensity transformation property of the target under the measurement.[14,34]

This polarization-diverse intensity image reflected the true backscattered signal intensity of the target without any influence of polarization or birefringence.[22,23] Note that polarization-diverse S-OCT image could also be equivalently calculated only by a summation of one of two columns of the 2 × 2 Jones-matrix S-OCT when negligible diattenuation could be assumed. It has been used as a reasonable implementation of the polarization-diverse S-OCT when advanced polarization contrast, such as the local retardation, is not required.

Third, the local retardation that represented a magnitude of birefringence per unit depth was calculated, which is shown as a false-color map (see Fig. 1C). It was calculated from the localized Jones matrix along the depth to resolve cumulative effect of birefringence along the depth. The details were described previously.[32,34] In this study, the local retardation image was referred as PS-OCT for simplicity, because other advanced contrast related to polarization was not used.

All the calculations of the signal intensity are performed in a linear scale, and the results are presented in a logarithmic scale for visualization.

Image Reading Procedures

Anatomic structures of the anterior chamber angle were defined according to the previous studies[10,35]; the scleral spur, the point where there was a change in curvature in the corneoscleral - aqueous interface, often appearing as an inward protrusion of the sclera; Schwalbe's line, the point where the anterior end of TM meets the peripheral end of the corneal endothelium; and SC, a tubular canal located at the sclerocorneal junction. The TM was bordered by the scleral spur, the posterior end point of the SC, and Schwalbe's line. The BELL was defined as a hyporeflective (S-OCT) or high birefringent (PS-OCT) band wrapping around the TM and SC.[10]

The OCT images of nasal and temporal anterior chamber angles were reviewed by two trained graders (authors Y.U. and H.M.) independently without any knowledge of the participant's clinical characteristics. Horizontal angles were selected as in a previous study,[10] because vertical angles were difficult to measure in some cases because of the presence of eyelids. The graders were allowed to change the intensity and contrast of the images to maximize visualization. The graders rated visibility (N = not visible and Y = visible) for each angle landmark; TM, SC, and BELL. In the evaluation of 2 × 2 Jones-matrix S-OCT images, visibility was judged to be positive if the structure was detected on at least one image out of four images.

Statistical Analysis

Considering the detection rate of TM (approximately 62–81%), SC (approximately 25–52%), and BELL (approximately 82–98%) in a previous study,[10] a sample size of 70 eyes was calculated to be enough to detect the difference among groups ($\alpha = 0.05$, power = 80%). Numerical data are expressed as mean ± standard deviation. Statistical comparisons between two groups were performed using the Mann-Whitney U test. The categorical data were compared between groups with the χ^2 test or the Fisher's exact test. The prevalence-adjusted bias-adjusted kappa value (κ value; PABAK) was calculated for evaluation of intergrader agreement.[36] A κ value of 0.2 or less was defined as poor agreement, a κ value between 0.20 and 0.40 was defined as fair agreement, a κ value between 0.41 and 0.60 was defined as moderate agreement, a κ value between 0.61 and 0.80 was defined as good agreement, and a κ value of more than 0.8 was defined as excellent agreement.[37] Statistical analysis was performed using SPSS Statistics for Windows software (version 27; IBM Corp., Armonk, NY, USA). A P value of less than 0.05 was considered statistically significant.

Results

A total of 97 eyes of 55 subjects were included in the study. Among them, there were 65 eyes of 37 patients with glaucoma (male/female patients = 22/15, 66.6 ± 13.9 years old) and 32 eyes of 18 healthy volunteers (male/female volunteers = 9/9, 51.0 ± 17.3 years old). The glaucoma group included 40 eyes with primary open angle glaucoma, 11 eyes with exfoliation glaucoma, 9 eyes with secondary glaucoma, 4 eyes with normal tension glaucoma, and 1 eye with primary angle closure glaucoma. Among the eyes with secondary glaucoma, 7 eyes were due to uveitis with open angle, and 2 eyes had neovascular glaucoma with open angle in one eye and closed angle in another eye.

Figure 1 shows three forms of OCT images of a representative case. In the 2 × 2 Jones-matrix S-OCT image (see Fig. 1A), artificial vessel-like structures and hyporeflective bands are found in the sclera, that correspond to the artifacts produced by local birefringence. BELL-like structure (arrow) and TM (arrow head) are visible. In the PS-OCT image (see Fig. 1C), BELL (arrow) and TM (arrow head) are observed. Figure 2 shows a set of S-OCT and PS-OCT images of another representative case with different visibility of the landmarks. Figure 3 is the images of an eye with a closed angle.

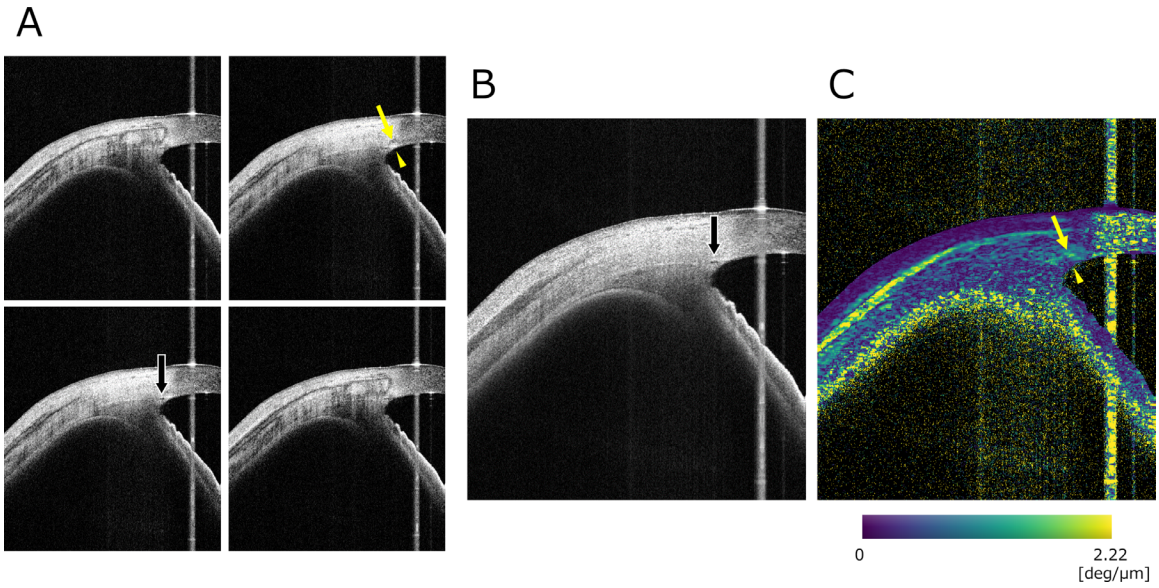

Figure 2. A set of scattering OCT (S-OCT) and polarization-sensitive OCT (PS-OCT). (**A**) In the 2 × 2 Jones-matrix S-OCT image, many artificial vessel-like structures and hyporeflective bands are found in the sclera, which correspond to the artifacts by local birefringence. Band of extracanalicular limbal lamina (BELL)-like structure (hyporeflective band-shaped area, *yellow arrow*), trabecular meshwork (TM) (surrounded by BELL, *arrow head*), and Schlemm's canal (SC) (hyporeflective liner area, *black arrow*) are visible. (**B**) In polarization-diverse S-OCT image, SC (black arrow) is observed. (**C**) In PS-OCT image, BELL (high birefringence band-shaped area, *arrow*) and TM (low birefringence area surrounded by BELL, *arrow head*) are identified.

The visibility of angle landmarks is summarized in Figure 4. The detection rate of TM and BELL was significantly higher with PS-OCT and 2 × 2 Jones-matrix S-OCT than with polarization-diverse S-OCT, indicating the influence of an artifact caused by local birefringence on 2 × 2 Jones-matrix S-OCT measurements. SC was difficult to visualize with any modalities. The intergrader agreements are summarized

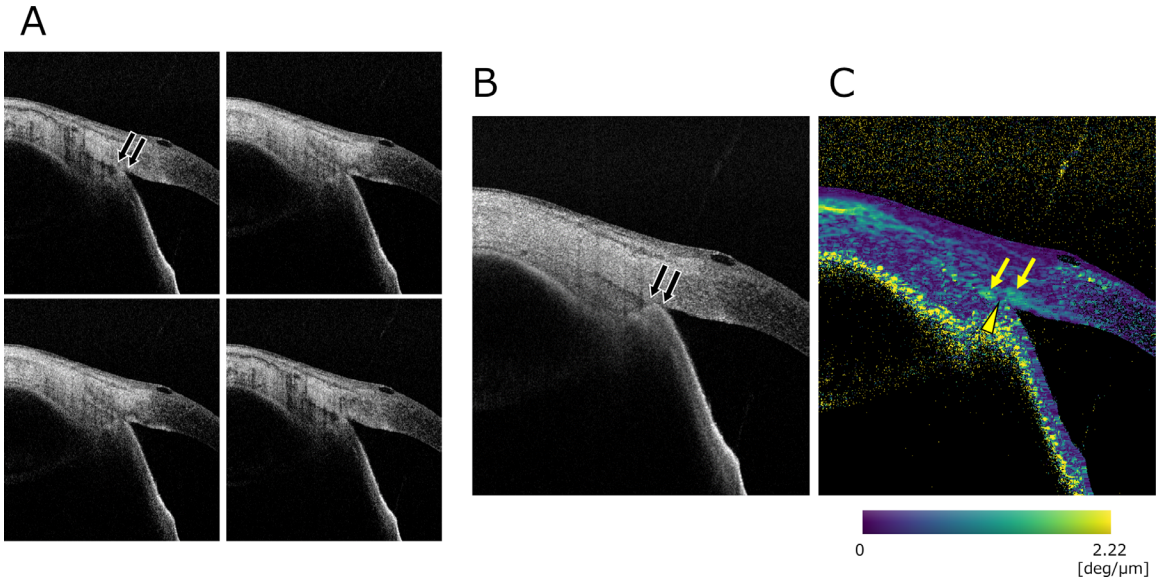

Figure 3. Images of an eye with completely closed angle. In the 2 × 2 Jones-matrix scattering OCT (S-OCT) image (**A**) and polarization-diverse S-OCT image (**B**), peripheral anterior synechia (black arrow) is observed. Angle structures are difficult to identify due to the artifacts by local birefringence. (**C**) In polarization-sensitive OCT (PS-OCT) image, BELL (high birefringence band-shaped area, arrow) and TM (low birefringence area surrounded by BELL, *arrow head*) are recognized. The location of TM indicates the presence of high peripheral anterior synechia.

Table 1. Visibility of Angle Landmarks and Intergrader Agreement

	Grader 1 (194 Angles)	Grader 2 (194 Angles)	Prevalence-Adjusted Bias-Adjusted κ Value
2 × 2 Jones-matrix S-OCT			
Trabecular meshwork	130 (67.0%)	146 (75.3%)	0.65
Schlemm's canal	31 (16.0%)	24 (12.4%)	0.56
BELL	171 (88.1%)	173 (89.2%)	0.88
Polarization-diverse S-OCT			
Trabecular meshwork	65 (33.5%)	64 (33.0%)	0.33
Schlemm's canal	30 (15.5%)	28 (14.4%)	0.61
BELL	33 (17.0%)	64 (33.0%)	0.31
PS-OCT			
Trabecular meshwork	179 (92.3%)	190 (97.9%)	0.82
Schlemm's canal	1 (0.5%)	0 (0.0%)	0.99
BELL	193 (99.5%)	192 (99.0%)	0.97

S-OCT, scattering optical coherence tomography; BELL, band of extracanalicular limbal lamina; PS-OCT, polarization-sensitive optical coherence tomography.

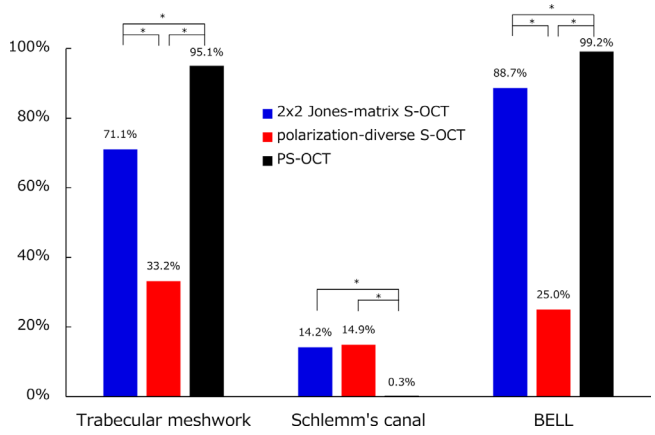

Figure 4. Visibility of anterior chamber angle landmarks in a total of 388 images evaluated by two graders using three OCT modalities. *P < 0.001. S-OCT: scattering optical coherence tomography, PS-OCT: polarization-sensitive optical coherence tomography, BELL: band of extracanalicular limbal lamina.

in Table 1. The PABAK value was moderate with 2 × 2 Jones-matrix and polarization-diverse OCT, and excellent with PS-OCT.

Visibility of anterior chamber angle landmarks was compared between eyes with glaucoma and healthy eyes (Table 2). With polarization-diverse S-OCT, the rate of visibility of TM ($P = 0.002$) and SC ($P < 0.001$) was significantly lower in eyes with glaucoma than in normal eyes. With PS-OCT, the rate of visibility of TM was significantly lower in eyes with glaucoma than in normal eyes ($P = 0.003$).

Discussion

We found that BELL-like structure was visible in 88.7% of images with 2 × 2 Jones-matrix S-OCT, in agreement with 95% visibility of BELL with the conventional S-OCT.[10] This observation, however, seems to be influenced by the artifacts arising from local birefringence since the detection rate of BELL was only 25% with polarization-diverse S-OCT. On the other hand, BELL was identified in 99.2% of cases with PS-OCT in the present study. In pathology, BELL was observed as avascular area of collagenous layers external to SC, in which tightly packed collagen fibrils may provide limbal support to the eye and angle structures.[10] Because of such anatomic features, BELL can be a strong source of local birefringence, which theoretically is best observed with PS-OCT. Conventional intensity OCT does not provide a tissue-specific contrast, causing an ambiguity with image interpretation in several cases. In contrast, PS-OCT can analyze form birefringence observed in fibrous tissues that contain collagens with specific polarization properties.

Trabecular meshwork was visible in 95.1% of images with PS-OCT, whereas only in 71.1% with 2 × 2 Jones-matrix S-OCT and 33.2% with polarization-diverse OCT. Because TM is a collagenous tissue with a perforate structure, the meshwork shows birefringence and can be well visualized with PS-OCT.[38,39] Yasuno et al.[14] compared S-OCT and PS-OCT in visualizing TM, and showed a significant improvement of visibility with PS-OCT. In their study, three graders rated the visibil-

Table 2. Comparison of Visibility of Angle Landmarks Between Glaucomatous and Healthy Eyes

	Glaucoma (260 Angles)	Normal (128 Angles)	*P* Value
2 × 2 Jones-matrix S-OCT			
Trabecular meshwork	178 (68.5%)	98 (76.6%)	0.098
Schlemm's canal	31 (11.9%)	24 (18.8%)	0.070
BELL	227 (87.3%)	117 (91.4%)	0.101
Polarization-diverse S-OCT			
Trabecular meshwork	73 (28.1%)	56 (43.8%)	0.002
Schlemm's canal	25 (9.6%)	33 (25.8%)	<0.001
BELL	56 (21.5%)	41 (32.0%)	0.187
PS-OCT			
Trabecular meshwork	243 (93.5%)	128 (100%)	0.003
Schlemm's canal	1 (0.4%)	0 (0%)	0.483
BELL	257 (98.8%)	128 (100%)	0.222

S-OCT, scattering optical coherence tomography; BELL, band of extracanalicular limbal lamina; PS-OCT, polarization-sensitive optical coherence tomography.

ity of TM using a four-leveled grading system, and intergrader agreement, intermodality differences, and interquadrant dependence of visibility were statistically examined. It was found that all three combinations of graders show substantial agreement in visibility with PS-OCT (ρ = 0.74, 0.70, and 0.68, Spearman's correlation), whereas only one of three shows substantial agreement with S-OCT (ρ = 0.72). In the present study, we also found that the intergrader agreement coefficient was highest with PS-OCT (see Table 1), indicating the usefulness of PS-OCT in the observation of anterior chamber angle landmarks including BELL and TM.

Schlemm's canal was more difficult to visualize than TM and BELL with any of the three OCT modalities. Crowell et al.[10] reported lower visibility of SC (40%) than BELL (95%) and TM (73%). McKee et al.[40] described that scleral spur, Schwalbe's line, and SC were visible with high-density scan of a swept-source OCT in 95% to 100%, 68% to 98%, and 12% to 42% of normal subjects, respectively. The visibility was reduced in low-density images to 50% to 95%, 0% to 10%, and 0%, respectively. Thus, visualization of SC in living eyes is quite challenging even with the modern OCT technologies. In addition, because SC is a hollow space (tubular canal) rather than a solid collagenous tissue, PS-OCT is not suitable at all for its observation.

Visibility of TM with 2 × 2 Jones-matrix S-OCT, polarization-diverse S-OCT, and PS-OCT was 71.1%, 33.2%, and 95.1%, respectively. Because the current graders located TM as the hyper-reflective area surrounded by BELL-like structure with 2 × 2 Jones-matrix S-OCT or low birefringence area surrounded by BELL with PS-OCT, it seems that the high visibility rate of BELL with those modalities helped increase the detection rate of TM.

The visibility rates of TM and SC were lower in eyes with glaucoma than in healthy eyes. Previous studies indicated that SC areas were significantly smaller in patients with glaucoma than in healthy subjects.[41,42] Another study demonstrated that an open angle was associated with better visibility of angle landmarks on anterior segment OCT.[10] It was postulated that this may have to do with a decrease in the crowding of the angle with an open-angle configuration, which may allow the light to reflect better on the different structures. Different visibility of angle landmarks between glaucoma and healthy eyes may be attributed to such anatomical differences, but further studies are needed to elucidate the exact mechanisms.

In this study, we evaluated the intergrader agreement with the PABAK value, rather than the conventional Cohen's κ value. It is reported that in the presence of low disease prevalence, the κ statistic should be interpreted with caution.[36] A highly skewed distribution of agreements (e.g. most agreements in the same cell of a 2 × 2 table due to a very low prevalence of the clinical sign) will result in a very low κ value regardless of a high proportion of agreement among observers.[43,44] In general, κ values increase with an increased bias, and low prevalence results in a decrease in κ values. In most cases, bias is not a major problem. However, the low prevalence level results in a substantial reduction in κ values, which can be misleading. In case of low disease prevalence, PABAK is a useful indicator for measuring observer agreement. This is an adjusted measure that aims to alleviate the effect of bias and prevalence on κ values.

This study has some limitations. First, we evaluated only nasal and temporal angle structures, and other quadrants were not investigated. Second, although we demonstrated that PS-OCT can identify BELL in almost all cases, we cannot clearly state the structural or physiological significance of this structure. Further studies are awaited.

In conclusion, we investigated the visibility of anterior chamber angle structures (TM, SC, and BELL) with three OCT modalities; 2 × 2 Jones-matrix S-OCT, polarization-diverse S-OCT, and PS-OCT. It was found that PS-OCT offered significantly higher identification rate of BELL and TM that are rich in collagen fibers than 2 × 2 Jones-matrix S-OCT and polarization-diverse S-OCT. In contrast, visualization of SC was more difficult with any OCT modalities. The visibility rate of TM and SC was lower in eyes with glaucoma than in healthy eyes.

Acknowledgments

Disclosure: **Y. Ueno**, None; **H. Mori**, None; **K. Kikuchi**, None; **M. Yamanari**, Tomey Corporation (E); **T. Oshika**, None

* YU and HM equally contributed to this work.

References

1. Goel M, Picciani RG, Lee RK, Bhattacharya SK. Aqueous humor dynamics: a review. *Open Ophthalmol J*. 2010;4:52–59.
2. Costagliola C, dell'Omo R, Agnifili L, et al. How many aqueous humor outflow pathways are there? *Surv Ophthalmol*. 2020;65(2):144–170.
3. Gao K, Li F, Aung T, Zhang X. Diurnal variations in the morphology of Schlemm's canal and intraocular pressure in healthy Chinese: An SS-OCT study. *Invest Ophthalmol Vis Sci*. 2017;58(13):5777–5782.
4. Zhao Y, Chen J, Yu X, Xu J, Sun X, Hong J. Age-related changes in human Schlemm's canal: An in vivo optical coherence tomography-based study. *Front Physiol*. 2018;9:630.
5. Chen Z, Sun J, Li M, et al. Effect of age on the morphologies of the human Schlemm's canal and trabecular meshwork measured with swept–source optical coherence tomography. *Eye (Lond)*. 2018;32(10):1621–1628.
6. Qiao Y, Tan C, Zhang M, Sun X, Chen J. Comparison of spectral domain and swept source optical coherence tomography for angle assessment of Chinese elderly subjects. *BMC Ophthalmol*. 2019;19(1):142.
7. Fernández-Vigo JI, Kudsieh B, De-Pablo-Gómez-de-Liaño L, et al. Schlemm's canal measured by optical coherence tomography and correlation study in a healthy Caucasian child population. *Acta Ophthalmol*. 2019;97(4):e493–e498.
8. Jing S, Chen Z, Chen W, Zhang H, Wang J. The 360° circumferential opening of Schlemm's canal in normal individuals detected by enhanced depth imaging optical coherence tomography. *Medicine (Baltimore)*. 2020;99(7):e19187.
9. Abdeen W, Esmael AF, Gawdat G, El-Fayoumi D. Anterior chamber angle features in primary congenital glaucoma infants using hand-held anterior segment-oct. *Eye (Lond)*, https://doi.org/10.1038/s41433-021-01583-1. Epub ahead of print.
10. Crowell EL, Baker L, Chuang AZ, et al. Characterizing anterior segment OCT angle landmarks of the trabecular meshwork complex. *Ophthalmology*. 2018;125(7):994–1002.
11. Kagemann L, Wollstein G, Ishikawa H, et al. Identification and assessment of Schlemm's canal by spectral-domain optical coherence tomography. *Invest Ophthalmol Vis Sci*. 2010;51(8):4054–4059.
12. Gold ME, Kansara S, Nagi KS, et al. Age-related changes in trabecular meshwork imaging. *Biomed Res Int*. 2013;2013:295204.
13. Fernández-Vigo JI, García-Feijóo J, Martínez-de-la-Casa JM, García-Bella J, Fernández-Vigo JA. Morphometry of the trabecular meshwork in vivo in a healthy population using fourier-domain optical coherence tomography. *Invest Ophthalmol Vis Sci*. 2015;56(3):1782–1788.
14. Yasuno Y, Yamanari M, Kawana K, et al. Visibility of trabecular meshwork by standard and polarization-sensitive optical coherence tomography. *J Biomed Opt*. 2010;15(6):061705.
15. Yamanari M, Lim Y, Makita S, Yasuno Y. Visualization of phase retardation of deep posterior eye by polarization-sensitive swept-source optical coherence tomography with 1-microm probe. *Opt Express*. 2009;17(15):12385–12396.
16. Collett E. Mathematical formulation of the interference laws of Fresnel and Arago. *Am J Physics*. 1971;39:1483–1495.
17. Barakat R. Analytic proofs of the Arago–Fresnel laws for the interference of polarized light. *J Opt Soc Am A*. 1993;10:180–185.
18. Mujat M, Dogariu A, Wolf E. A law of interference of electromagnetic beams of any state of coherence and polarization and the Fresnel-Arago interference laws. *J Opt Soc Am A*. 2004;21:2414–2417.

19. Kazovsky LG. Phase- and polarization-diversity coherent optical techniques. *J Lightwave Technol*. 1989;7:279–292.
20. Herz P, Chen Y, Aguirre A, et al. Ultrahigh resolution optical biopsy with endoscopic optical coherence tomography. *Opt Express*. 2004;12(15):3532–3542.
21. Bouma BE, Yun SH, Vakoc BJ, Suter MJ, Tearney GJ. Fourier-domain optical coherence tomography: recent advances toward clinical utility. *Curr Opin Biotechnol*. 2009;20(1):111–118.
22. Baumann B. Polarization sensitive optical coherence tomography: A review of technology and applications. *Appl Sci*. 2017;7:474.
23. de Boer JF, Hitzenberger CK, Yasuno Y. Polarization sensitive optical coherence tomography - a review [Invited]. *Biomed Opt Express*. 2017;8(3):1838–1873.
24. Yasuno Y, Yamanari M, Kawana K, Oshika T, Miura M. Investigation of post-glaucoma-surgery structures by three-dimensional and polarization sensitive anterior eye segment optical coherence tomography. *Opt Express*. 2009;17(5):3980–3996.
25. Fukuda S, Beheregaray S, Kasaragod D, et al. Noninvasive evaluation of phase retardation in blebs after glaucoma surgery using anterior segment polarization-sensitive optical coherence tomography. *Invest Ophthalmol Vis Sci*. 2014;55(8):5200–5206.
26. Yamanari M, Tsuda S, Kokubun T, et al. Fiber-based polarization-sensitive OCT for birefringence imaging of the anterior eye segment. *Biomed Opt Express*. 2015;6(2):369–389.
27. Fukuda S, Fujita A, Kasaragod D, et al. Quantitative evaluation of phase retardation in filtering blebs using polarization-sensitive optical coherence tomography. *Invest Ophthalmol Vis Sci*. 2016;57(14):5919–5925.
28. Kasaragod D, Fukuda S, Ueno Y, Hoshi S, Oshika T, Yasuno Y. Objective evaluation of functionality of filtering bleb based on polarization-sensitive optical coherence tomography. *Invest Ophthalmol Vis Sci*. 2016;57(4):2305–2310.
29. Götzinger E, Pircher M, Dejaco-Ruhswurm I, Kaminski S, Skorpik C, Hitzenberger CK. Imaging of birefringent properties of keratoconus corneas by polarization-sensitive optical coherence tomography. *Invest Ophthalmol Vis Sci*. 2007;48(8):3551–3558.
30. Fukuda S, Yamanari M, Lim Y, et al. Keratoconus diagnosis using anterior segment polarization-sensitive optical coherence tomography. *Invest Ophthalmol Vis Sci*. 2013;54(2):1384–1391.
31. Fukuda S, Kishino G, Hoshi S, et al. Repeatability of corneal phase retardation measurements by polarization-sensitive optical coherence tomography. *Invest Ophthalmol Vis Sci*. 2015;56(5):3196–3201.
32. Yamanari M, Uematsu S, Ishihara K, Ikuno Y. Parallel detection of Jones-matrix elements in polarization-sensitive optical coherence tomography. *Biomed Opt Express*. 2019;10(5):2318–2336.
33. Kosugi M, Kokubun T, Tsuda S, Yamanari M, Nakazawa T. Usefulness of polarization-sensitive optical coherence tomography-derived attenuation-coefficient images to visualize the internal structure of the filtering bleb. *Curr Eye Res*. 2021;46(4):606–609.
34. Yamanari M, Tsuda S, Kokubun T, et al. Estimation of Jones matrix, birefringence and entropy using Cloude-Pottier decomposition in polarization-sensitive optical coherence tomography. *Biomed Opt Express*. 2016;7(9):3551–3573.
35. Cumba RJ, Radhakrishnan S, Bell NP, et al. Reproducibility of scleral spur identification and angle measurements using Fourier domain anterior segment optical coherence tomography. *J Ophthalmol*. 2012;2012:487309.
36. Mak HK, Yau KK, Chan BP. Prevalence-adjusted bias-adjusted kappa values as additional indicators to measure observer agreement. *Radiology*. 2004;232(1):302–303.
37. Altman DG. *Practical Statistics for Medical Research*. London, UK: Chapman and Hall; 1991.
38. Pircher M, Goetzinger E, Leitgeb R, Hitzenberger CK. Transversal phase resolved polarization sensitive optical coherence tomography. *Phys Med Biol*. 2004;49(7):1257–1263.
39. Yamanari M, Makita S, Yasuno Y. Polarization-sensitive swept-source optical coherence tomography with continuous source polarization modulation. *Opt Express*. 2008;16(8):5892–5906.
40. McKee H, Ye C, Yu M, Liu S, Lam DS, Leung CK. Anterior chamber angle imaging with swept-source optical coherence tomography: detecting the scleral spur, Schwalbe's Line, and Schlemm's Canal. *J Glaucoma*. 2013;22(6):468–472.
41. Kagemann L, Wollstein G, Ishikawa H, et al. Identification and assessment of Schlemm's canal by spectral-domain optical coherence tomography. *Invest Ophthalmol Vis Sci*. 2010;51(8):4054–4059.
42. Hong J, Xu J, Wei A, et al. Spectral-domain optical coherence tomographic assessment of Schlemm's canal in Chinese subjects with primary open-angle glaucoma. *Ophthalmology*. 2013;120(4):709–715.
43. Byrt T, Bishop J, Carlin JB. Bias, prevalence and kappa. *J Clin Epidemiol*. 1993;46(5):423–429.
44. Lantz CA, Nebenzahl E. Behavior and interpretation of the kappa statistic: resolution of the two paradoxes. *J Clin Epidemiol*. 1996;49(4):431–434.